Space Weather

RESEARCH ARTICLE
10.1029/2021SW002744

On the Properties of and Ionospheric Conditions Associated With a Mid-Latitude Scintillation Event Observed Over Southern United States

F. S. Rodrigues[1], J. G. Socola[1], A. O. Moraes[2], C. Martinis[3], and D. A. Hickey[4]

[1]W. B. Hanson Center for Space Sciences, The University of Texas at Dallas, Richardson, TX, USA, [2]Instituto de Aeronautica e Espaco, IAE, São Paulo, Brazil, [3]Center for Space Physics, Boston University, Boston, MA, USA, [4]Space Science Division, U. S. Naval Research Laboratory, Washington, DC, USA

Key Points:

- We present and discuss the detection of L-Band ionospheric scintillations that occurred over southern United States
- The severity and temporal properties of the observed scintillations are similar to those of events associated with equatorial plasma bubbles
- A modest geomagnetic storm prompted extreme background ionospheric conditions and perturbations leading to the observed scintillations

Correspondence to:
F. S. Rodrigues,
fabiano@utdallas.edu

Citation:
Rodrigues, F. S., Socola, J. G., Moraes, A. O., Martinis, C., & Hickey, D. A. (2021). On the properties of and ionospheric conditions associated with a mid-latitude scintillation event observed over southern United States. *Space Weather*, *19*, e2021SW002744. https://doi.org/10.1029/2021SW002744

Received 19 FEB 2021
Accepted 4 JUN 2021

Abstract While low and high-latitude ionospheric scintillation have been extensively reported, significantly less information is available about the properties of and conditions leading to mid-latitude scintillations. Here, we report and discuss scintillation observations made in the Southern United States (UT Dallas, 32.99°N, 96.76°W, 43.2°N dip latitude) on June 1st, 2013. The measurements were made by a specialized dual-frequency GPS-based scintillation monitor which allowed us to determine main properties of this mid-latitude scintillation event. Additionally, simultaneous airglow observations and ionospheric total electron content (TEC) maps provided insight on the conditions leading to observed scintillations. Moderate amplitude scintillations (S_4>~0.4) occurred in both L1 and L2C signals, and severe (S_4 > ~0.8) events occurred in L2C signals at low (<30°) elevation angles. Phase scintillation accompanied amplitude fadings, with maximum σ_ϕ values exceeding 0.5 radians in L2C. We also show that the observed phase scintillation magnitudes increased with amplitude scintillation severity. Decorrelation times were mostly between 0.25 and 1.25 s, with mean value around 0.65 s for both L1 and L2C. Frequency scaling of S_4 matched fairly well the predictions of weak scattering theory but held for observations of moderate and strong amplitude scintillation as well. Scintillation occurred during the main phase of a modest magnetic storm that, nevertheless, prompted an extreme equatorward movement of the mid-latitude trough and large background TEC enhancements over the US. Scintillations, however, occurred within TEC and airglow depletions observed over Texas. Finally, scintillation properties including severity and rapidity, and associated TEC signatures are comparable to those associated with equatorial spread F.

Plain Language Summary The ionosphere is a region of the upper atmosphere characterized by a relatively large density of free ions and electrons created, in most part, by solar photoionization. Spatial and temporal variations in the ionospheric electron density cause the diffraction of radio waves such as those used by GPS. The diffraction of the radio waves, as a result, cause fluctuations in the amplitude and/or phase of signal measured by a ground-based receiver, for instance. These fluctuations are referred to as ionospheric scintillations. Ionospheric scintillations are commonly observed at low and high latitudes, where ionospheric irregularities are known to develop very frequently. Here, we report detailed observations of an ionospheric scintillation event that occurred on June 1st, 2013 over mid-latitudes (Southern United States) where scintillations are thought to occur very rarely. We were able to capture the event with a specialized scintillation monitor during an educational project. This fortunate observation provided details about the properties (severy, rapidity, frequency scaling, etc.) of the observed mid-latitude scintillations. The report provides new information about mid-latitude scintillation that is of interest to a better fundamental understanding of ionospheric irregularities and their impact on signals in the frequency band used by global navigation satellite systems (GPS, Galileo, BeiDou, etc.).

1. Introduction

Ionospheric radio scintillation refers to rapid fluctuations observed in the amplitude or phase of trans-ionospheric radio signals and caused by temporal and spatial irregularities in the density of the ionospheric plasma (Yeh & Liu, 1982). These irregularities cause significant changes in the permittivity of the propagation environment (ionospheric plasma) and diffraction (or refraction) of radio waves propagating through

this medium. Diffractive effects are particularly important as they can produce fast phase variations and power fades exceeding 30 dB. These effects can affect the performance of technological assets such as global navigation satellite systems (GNSS) (P. M. Kintner et al., 2007).

Theoretical efforts have been dedicated to a better understanding of wave propagation in random media (e.g., Rino, 1976; Yeh & Liu, 1982). This is the idealized case of radio signals transmitted from satellites and propagating through a turbulent ionospheric plasma filled with a broad spatial spectrum of irregularities in electron density (or refractive index). It can be shown that for a signal of wavelength "λ" and a scattering medium located at a distance "r" above an observation plane, irregularities with scale sizes around the Fresnel radius ($r_F = \sqrt{2\lambda r}$) contribute the most to the observed spatial patterns of amplitude scintillation (Yeh & Liu, 1982). Therefore, the observed scintillation pattern depends on the Fresnel radius, the drift speed of the ionospheric irregularities, and the relative velocity between receiver and signal transmitter.

Ionospheric scintillation is commonly classified according to the magnetic latitude of its occurrence and divided into low (or equatorial), middle and high latitude scintillation (Aarons, 1982).

Low latitude scintillation events refer to those occurring within approximately ±20° magnetic (dip) latitude. Dip latitude (λ_{dip}) is defined in terms of local magnetic inclination (I), where $\lambda_{dip} = \tan^{-1}\left(\tan\left(I\right) / 2\right)$ (Laundal & Richmond, 2017). The ionospheric irregularities responsible for the diffraction of the radio waves at low latitudes associated with equatorial spread F (ESF). ESF is the name often used to describe a broad range of irregularities that develop in the nighttime equatorial F-region under the ionospheric Generalized Rayleigh-Taylor (GRT) instability. The GRT instability is thought to be responsible for the development of large-scale (several 10s of km) electron density structures. These large-scale structures then produce conditions for the development of secondary plasma instabilities capable of creating smaller scale irregularities and scintillation (Woodman, 2009). The severity of amplitude scintillation increases with the absolute magnitude of the ionospheric density perturbations (Basu et al., 1976). Therefore, the increased background ionospheric density at low latitudes, associated with the equatorial anomaly (Appleton, 1946), is known to provide conditions for the frequent occurrence of severe scintillation events (e.g., de Paula et al., 2003).

High latitude scintillation refers to events observed in the auroral oval and polar cap, which are predominantly beyond (poleward) of approximately ±60° dip latitude. High latitude scintillation have often been associated with large horizontal ionospheric gradients created by polar cap patches. Structuring and irregularities causing scintillation would be created by the gradient drift instability on the trailing edges of the patches (Buchau et al., 1985; Basu et al., 1998). Auroral electron precipitation and auroral arcs can also produce large density gradients and, presumably, ionospheric scintillation (P. M. Kintner et al., 2007).

Finally, the mid-latitude region covers the remaining latitudinal band, between ∼20° and 60° dip latitude. Until recently, however, the mid-latitude ionosphere had been assumed to be devoid of significant disturbances and irregularities (Erickson, 2020; Hysell et al., 2018; P. M. Kintner et al., 2007). Therefore, the effects of mid-latitude scintillation had also been thought to be of minimal effect on systems (Aarons, 1997).

The original view of a quiet ionosphere at mid latitudes led observational and theoretical efforts to focus predominantly on studies of ionospheric irregularities and scintillation at low and high latitudes. Recent advances in observational techniques and in the use of signals of opportunity for ionospheric measurements, however, allowed more observations at mid latitudes than previously possible. This is the case, for instance, of the use of existing geodetic networks of dual-frequency GPS receivers for measurements of ionospheric total electron content (TEC), generation of global and regional maps of vertical TEC and the development of assimilative models of ionospheric electron density (Bust & Mitchell, 2008; Komjathy, 1997). These GPS-based TEC measurements provided observational evidence of ionospheric disturbances at mid-latitudes occurring more often than previously thought (P. M. Kintner et al., 2008).

Adequate observations of ionospheric scintillation, however, require measurements of amplitude and/or phase of the probing radio signals at a high rate, typically >10 Hz. While a large number of geodetic GPS receivers exist and their observations are made publicly available, they only provide observables at a lower sampling rate, usually at 1/30 Hz and more recently at 1 Hz (Mrak et al., 2020). While geodetic receivers can provide some indication of the occurrence of ionospheric irregularities and potential scintillation (Bhattacharyya et al., 2000; Luo et al., 2020; Mrak et al., 2020; Pi et al., 1997), high rate measurements are needed

for proper specification of scintillation (Beach & Kintner, 1999). Routine, dedicated high-rate observations of ionospheric scintillation using specialized scintillation receivers, however, remain extremely reduced in number.

While an increasing number of experimental studies have indicated the occurrence of large-scale ionospheric structures and conditions that could favor the development of scintillation at mid-latitudes (e.g., Aa et al., 2018, 2019; Cherniak & Zakharenkova, 2016; Liu et al., 2020; Ma & Maruyama, 2006; Sun et al., 2013), only a limited number of events were adequately observed by specialized L-Band scintillation monitors (e.g., Jean et al., 2017; Ledvina et al., 2002; Rodrigues et al., 2004; Spogli et al., 2009). The lack of adequate observations have not yet allowed us to properly determine the occurrence and properties of mid-latitude scintillation. One notable example of mid-latitude scintillation observation was presented by Ledvina et al. (2002), which reported the detection of intense GPS L1 scintillations at mid latitudes for the first time. The case was observed by accident when the authors were testing a scintillation monitor at Cornell University. Like the event reported by Ledvina et al. (2002), most of the reported scintillation cases have been associated with ionospheric disturbances that originated at high latitudes and extended into the mid-latitude region (e.g., Afraimovich et al., 2009; Spogli et al., 2009).

Here, we contribute with analyses of high-rate L1 and L2C observations of amplitude and phase scintillation and TEC behavior made by a specialized GPS-based scintillation monitor located at a mid-latitude location (UT Dallas, ~45°N dip lat) on June 1st, 2013. More specifically, we determine and discuss the main properties of the observed scintillation patterns. These properties include severity, rapidity and frequency scaling. Of particular importance is the fact that the scintillation event was observed over the southern United States, at magnetic latitudes that were expected to be well outside the reach of both low- and high-latitude ionospheric disturbances under most geomagnetic conditions. Furthermore, additional insights about the ionospheric conditions leading to the observed scintillation events were guided by nearly collocated 630.0 nm nightglow observations made by all-sky imager and maps of the vertical TEC over the US.

This report is presented as follows: In Section 2, we provide information about the instrumentation used for scintillation observations, details about measurements and analyses. In Section 3, we present and discuss the observations. Auxiliary observations are also presented and discussed. Finally, in Section 4, we summarize the main results and conclusions.

2. Observations and Analyses

As part of an educational initiative, a Connected Autonomous Space Environment Sensor—CASES was installed on the campus of The University of Texas at Dallas—UTD (32.99°N, 96.76°W, 43.2°N dip latitude). CASES is a dual-frequency software GPS receiver developed for monitoring ionospheric scintillation. The receiver was used by undergraduate students for hands-on experience with remote sensing observations in space sciences, particularly with ionospheric TEC measurements, which can be made with dual-frequency GPS receivers. The ionospheric scintillation event described in this report was captured during one of the periods when the CASES receiver was being operated and maintained by the students.

The CASES receiver is a software-defined GPS receiver for scientific studies and monitoring of space weather (Crowley et al., 2011; Deshpande et al., 2012; O'Hanlon et al., 2011). CASES is a dual-frequency receiver capable of tracking GPS L1 (1,575.42 MHz) and L2C (1,227.60 MHz) signals. Therefore, CASES is capable of estimating relative TEC from a linear combination of measurements (pseudo-range or pseudo-phase) made at L1 and L2C. Not all GPS satellites transmit the L2C signal and, therefore, TEC estimates are only possible for signals transmitted by part of the GPS constellation. TEC measurements are made at 1 Hz rate and only relative (phase-based) measurements provided by the CASES receiver were used in this study.

The CASES receiver also provides indices of amplitude scintillation (S_4) and phase scintillation (σ_ϕ), which are commonly used to determine the occurrence and evaluate the severity ionospheric scintillation. The S_4 index can be described as the ratio of the standard deviation of the signal power to the mean signal power computed over a period of time (e.g., P. M. Kintner et al., 2007). The σ_ϕ index, on the other hand, is defined as the standard deviation of the measured phase (e.g., Beach, 2006). Additionally, the monitor provides estimates of the decorrelation time (τ_0) for scintillating signals. The decorrelation time can be defined as the

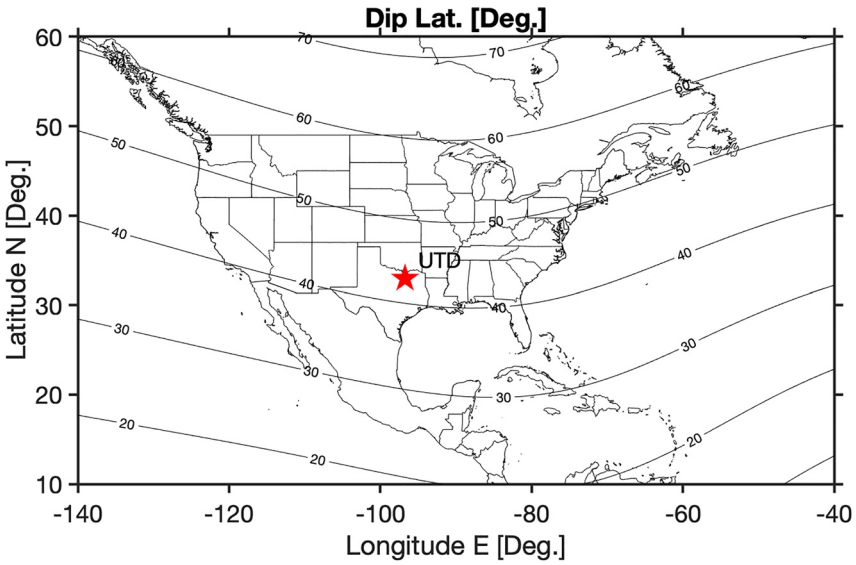

Figure 1. Map showing the location of the UTD CASES receiver (red star at 32.99°N, 96.76°W, 43.2°N dip latitude) whose observations were used in this study. Contour lines indicate dip latitude.

time lag at which a scintillating complex baseband signal's autocorrelation function falls off by a factor 1/e (e.g., Humphreys et al., 2010).

While S_4 and σ_ϕ are computed and stored at all times, τ_0 values are only computed and saved (along with 100 Hz in-phase and in-quadrature samples) during scintillation events. Scintillation events are defined based on the so-called "Scintillation Power Ratio" or SPR (O'Hanlon et al., 2011). SPR is a spectrum-based statistic that takes into consideration the behavior of both phase and amplitude of the observed signals.

Figure 1 shows the location of the CASES receiver. It also shows contours of dip latitude that serve to better illustrate that the receiver is located well within the mid-latitude region as defined by the geomagnetic field. Dip latitude was calculated using magnetic inclination provided by the International Geomagnetic Reference Field (IGRF) Model (Thébault et al., 2015).

3. Results and Discussion

Figure 2 provides an overview of the observations made on June 1st, 2013 by the UTD CASES receiver. Only observations for satellites with elevation greater than 20° are shown here to avoid some of the measurements that were affected by multipath and to show that scintillations were observed for ionospheric piercing points (IPPs) near the observation site. Panel (a) shows the magnitude of the amplitude scintillation (S_4 values) observed in the L1 and L2C signals. Panel (b) shows the magnitude of the phase scintillation (σ_ϕ values) observed on L1 and L2C signals. Panel (c) show the decorrelation times (τ_0) of observed amplitude scintillation patterns. Finally, panel (d) shows the relative slant TEC values estimated from the phase difference between L1 and L2C signals.

Figure 2 serves to show that both amplitude and phase scintillations were observed between 04:00 and 08:00 UT, that is, between 22:00 LT on May 31 and 02:00 LT on June 1. Figure 2 also serves to show that the scintillation events were accompanied by large fluctuations in TEC. Additional details about the measurements including specific characteristics and underlying conditions will be presented and discussed in the following sub-sections.

Figures 3 and 4 provide additional details about the observed scintillation events. They show individual time series of amplitude (Figure 3) and phase (Figure 4) scintillation data for each satellite observed around the time when scintillation events were detected, that is, between 04:00 and 08:00 UT. Note that now, for completeness, data for elevations greater than 10° are shown. Line-of-sight (slant) relative TEC values and the

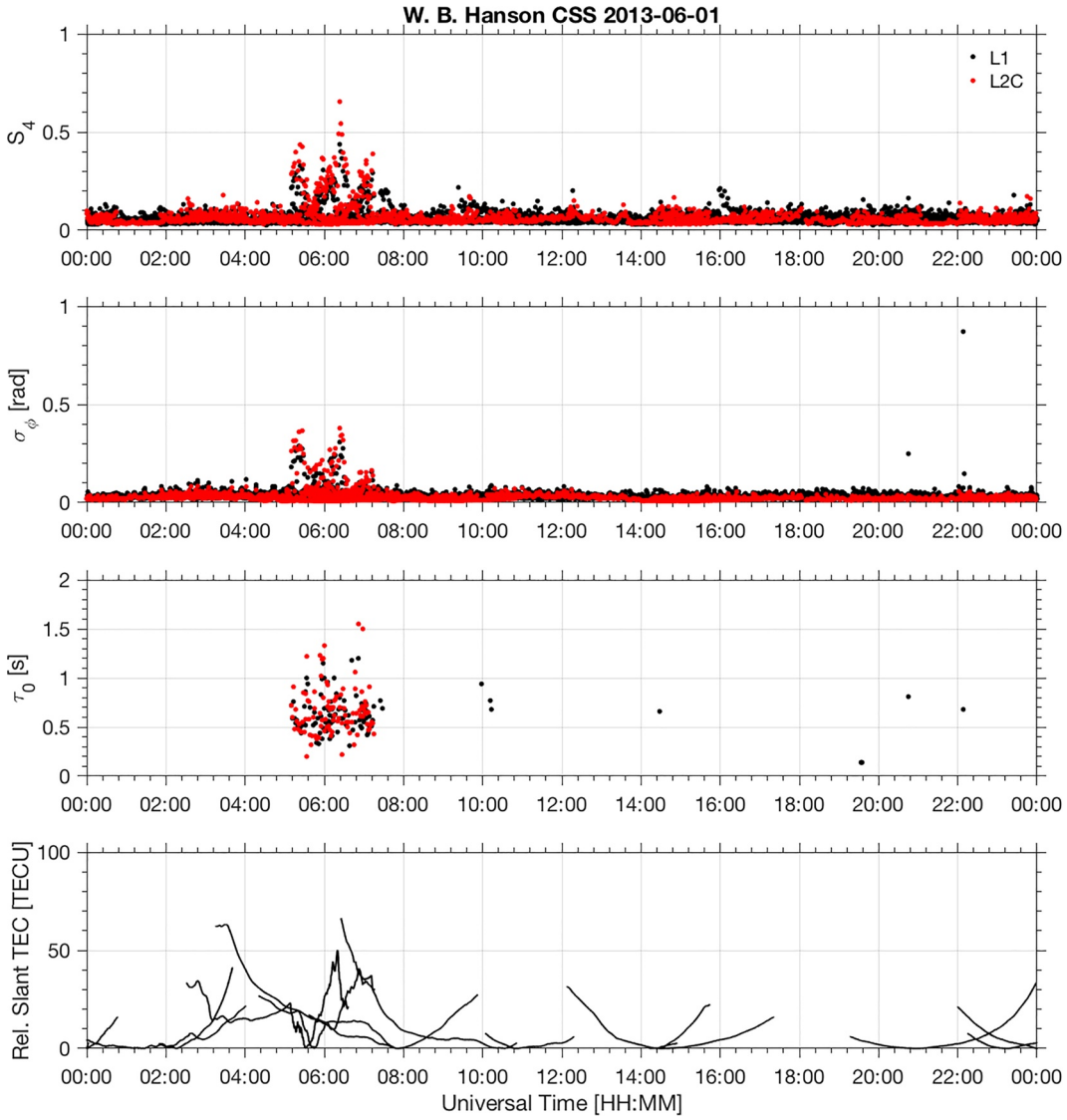

Figure 2. Observations of ionospheric scintillation made by the UTD CASES receiver on June 1st, 2013. The occurrence of scintillation and irregularities in TEC can be observed between 0400 UT and 0800 UT (UT = LT + 6 h). Only observations for satellites with elevation greater than 20° are shown.

variation of satellite elevation angle are also shown in each panel. TEC and L2C scintillation values are only available for those satellites transmitting both L1 and L2C signals, that is, SVIDs 5, 12, 15, 17, 24, 25, and 29.

Figure 3 serves to show that amplitude scintillation was observed in signals transmitted by various satellites, more noticeably on PRNs 12, 15, and 25. Additionally, Figure 4 shows that significant phase variations were also observed in the signals of the same satellites, concurrent to amplitude scintillation. We will focus on the characteristics of the perturbations detected on the signals of these satellites, that is, PRNs 12, 15, and 25, in the following presentation and discussion.

3.1. On the Severity of the Observed Scintillation Events

Figure 5 shows a closer look on the time series of scintillation magnitude and rapidity for PRNs 12, 15, and 25. It shows the variations in S_4 (top panels), σ_ϕ (middle panels) and τ_0 (bottom panels) for L1 and L2C signals.

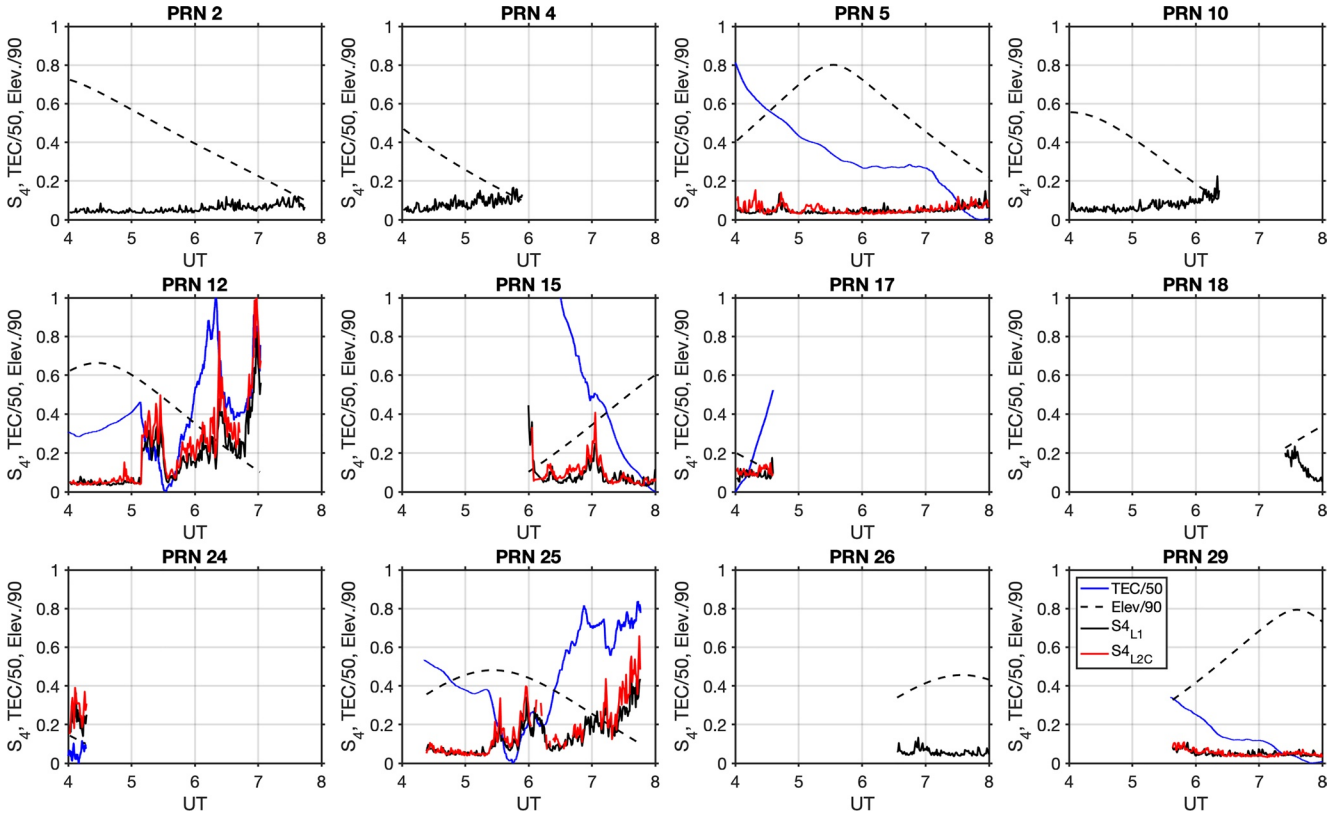

Figure 3. Observations of amplitude scintillation made by the UTD CASES receiver on June 1st, 2013 for each satellite in view (elevation > 10°) between 0400 and 0800 UT.

3.1.1. On the Observed Amplitude Scintillation

The most striking feature of the observations in Figure 5 is the occurrence of moderate and severe amplitude scintillation events on L1 and L2C signals. For elevation angles greater than 30°, amplitude scintillation is mostly weak, that is, $S_4 < \sim 0.4$. For elevation angles below about 30°, however, moderate ($S_4 > \sim 0.4$) scintillation events were observed in both L1 and L2C signals, and severe ($S_4 > \sim 0.8$) events were detected in the L2C signal transmitted by PRN 12.

Severe amplitude scintillation is mostly reported occurring at low magnetic latitudes, particularly near the equatorial anomaly peaks (around ± 15° dip latitude) where background ionospheric densities are elevated and ionospheric perturbations associated with ESF events have larger amplitudes (de Paula et al., 2003).

In order to provide a better perspective on the significance of the observed scintillation magnitudes, we look into a comprehensive survey of GPS scintillation measurements made in Sao Jose dos Campos, Brazil (17.3° dip latitude) reported by Moraes et al. (2017). Both amplitude and phase GPS scintillation measurements were made during ESF season (November 2014 to March 2015) in the Brazilian sector and showed an occurrence rate of only 1.91% (3.35%) of cases where $S_4 > 0.7$ for L1(L2C). The survey considered observations during times of most intense scintillation (20:00 and 23:00 LT) but from signals from satellites with elevation greater than 30°.

Therefore, our observations captured a mid-latitude event of amplitude scintillation that can be considered extreme even for low latitude conditions.

3.1.2. On the Observed Phase Scintillation

Figure 5 also shows that phase scintillation is observed concurrently with amplitude scintillation. Furthermore, it indicates that the magnitude of phase scintillation increases with the magnitude of amplitude

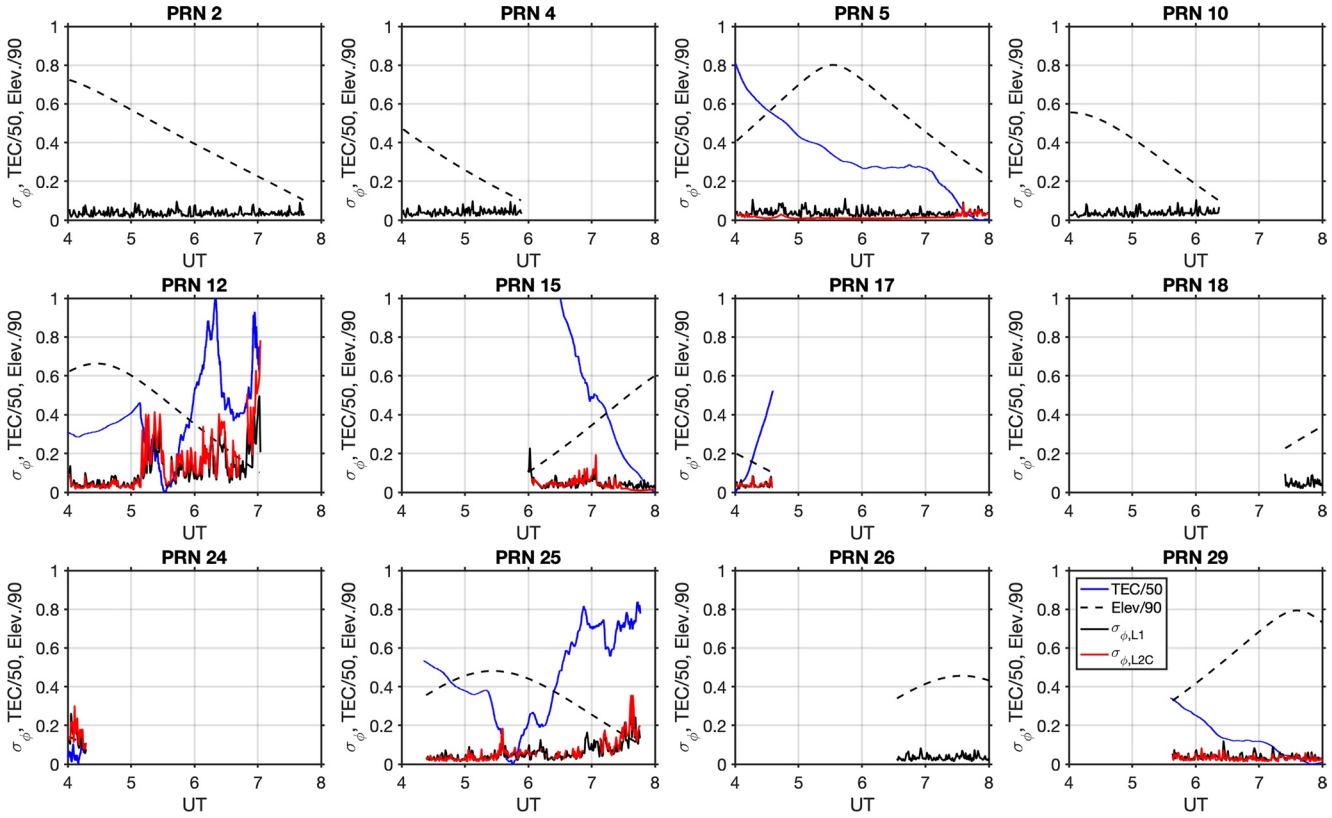

Figure 4. Observations of phase scintillation made by the UTD CASES receiver on June 1st, 2013 for each satellite in view (elevation > 10°) between 0400 and 0800 UT.

scintillation similarly to what was found in the study of low-latitude GPS L1 scintillation carried out by Carrano and Groves (2010) and in the comprehensive survey of L-Band (L1, L2, and L5) scintillation carried out by Moraes et al. (2017).

The relationship between σ_ϕ and S_4 is better quantified and illustrated in Figure 6. The top (bottom) panels show how σ_ϕ varies as a function of S_4 for L1 (L2C) and each PRN. The solid line in each panel shows a least squares estimate of a linear function (p) that best matches the observations. The expression for the linear functions are also shown in each panel. We must point out that while the data and results in Figure 6 serve to show that σ_ϕ does increase with S_4, the limited number of observations limit the reliability of the fits and derived relationships.

Finally, and more importantly, the survey of low-latitude scintillation carried out by Moraes et al. (2017) also showed that L1(L2C) phase scintillation with $\sigma_\phi > \sim 0.5$ rad occurred in only 1.00% (1.36%) of the observations. The histograms presented by Carrano and Groves (2010), however, indicate much higher occurrence rates of $\sigma_\phi > \sim 0.5$ rad in their observations. This is, presumably, caused by differences in solar flux conditions. The observations analyzed by Moraes et al. (2017) observations were made in between November of 2014 and March of 2015 when solar flux conditions were comparable to those of our 2013 mid-latitude measurements. The observations analyzed by Carrano and Groves (2010), however, were made during the much higher solar flux conditions of 2002.

Therefore, our observations captured a mid-latitude ionospheric irregularity event that produced cases of severe scintillation in both phase and amplitude.

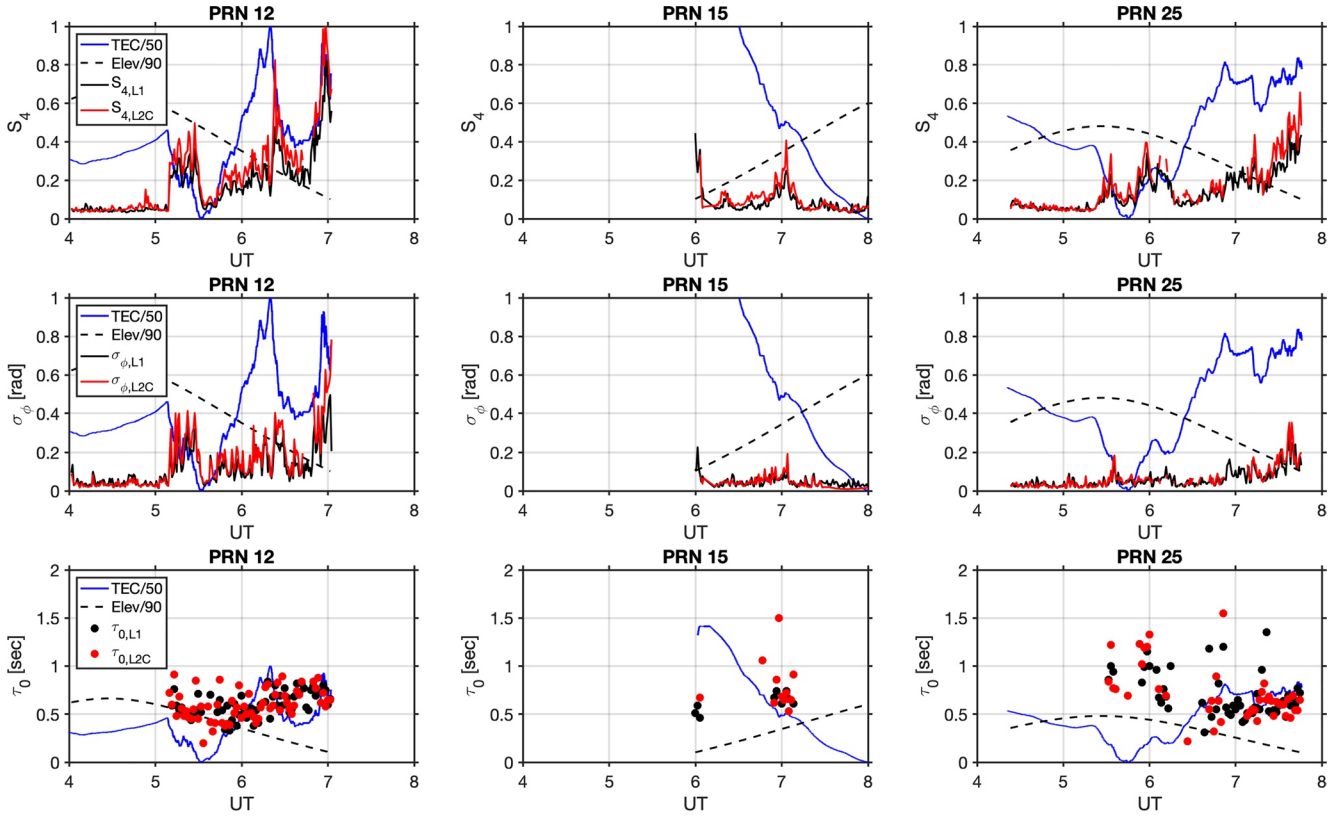

Figure 5. Summary of scintillation parameters (S_4, σ_ϕ, and τ_0) estimated by the CASES receiver for GPS PRNs 12 (left column), 25 (middle column) and 15 (right column) for the event of June 1, 2013.

3.2. On the Rapidity of the Observed Scintillations

We now comment on the rapidity of the observed amplitude scintillations. The decorrelation time (τ_0) provides a useful metric describing the temporal variation of the amplitude fluctuations caused by ionospheric irregularities.

In addition to magnitude, the temporal scale of the amplitude fluctuations can play a role in the performance of GNSS receivers. For instance, receiver tracking loops might have difficulties during cases of long duration signal fading events (Kintner et al., 2001; Ledvina et al., 2004). The decorrelation time also provides useful insight on the behavior of the irregularities responsible for scintillation since it is controlled by the Fresnel length and the relative velocity between the irregularities (irregularity drift) and the speed of the path of the signal as the GPS satellite moves across the sky. When the relative velocity is large, short decorrelation times are observed. On the other hand, when small relative velocities occur (velocity match or resonance), long duration fading events develop.

Using GPS-based spaced-receiver observations of low-latitude scintillations made in Cachoeira Paulista, Brazil (13°S dip lat) in November 1998, Kintner et al. (2001) showed examples of the linear relationship between scintillation pattern velocity and the velocity estimated from the ratio of Fresnel length and decorrelation time (fading rate). They showed, in particular, an illustrative example of low-latitude ESF scintillation where decorrelation times varied from ~1.0 s, when both irregularities and signal IPP traveled in the direction but with a relative velocity of about 100 m/s, to values over 4.0 s when the velocities of irregularities and signal IPP nearly matched. Then, when the irregularities and IPP moved in opposite directions maximizing the relative velocity at about 200 m/s, decorrelation times were ~0.5 s.

Figure 7 shows the observations and distribution of τ_0 values for L1 (top) and L2C (bottom). It serves to show that decorrelation times are mostly between 0.25 and 1.0 s with only a few cases outside this range.

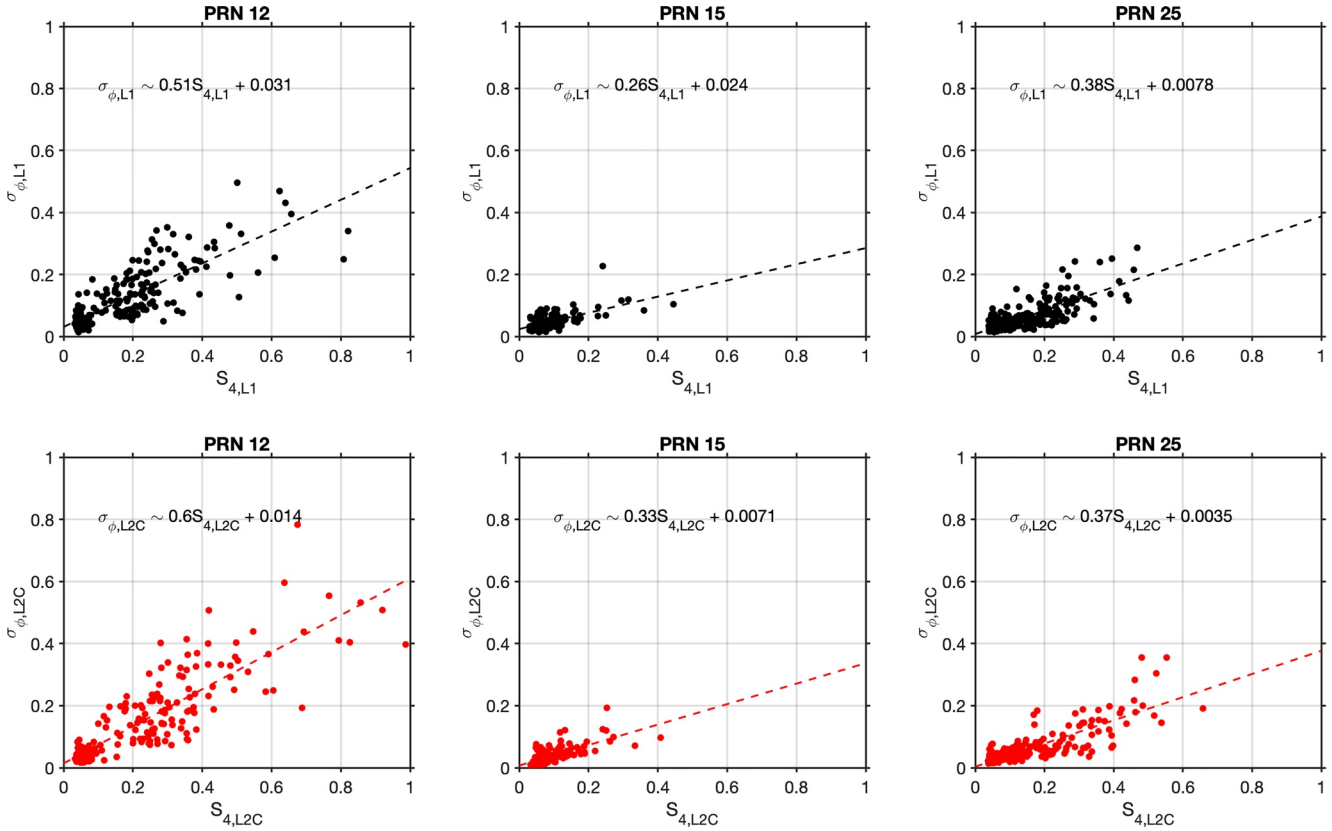

Figure 6. Variation of σ_ϕ as a function of S_4 for L1 (top panels) and L2C (bottom panels) transmitted by PRNs 12, 25, and 15.

Carrano and Groves (2010) also analyzed the temporal scales of GPS L1 amplitude scintillations measured during March 2002 by a receiver located in Ascension Island, a low latitude site (12.45°S). They showed that, for cases of $S_4 > 0.3$, the decorrelation times varied from ~0.4 to ~1.0 s. Additionally, Moraes et al. (2013) also analyzed one entire month worth of GPS L1 observations of amplitude scintillation made between December 14, 2001 and January 14, 2002 by a receiver in Sao Jose dos Campos, Brazil (17.5°S dip). They found mean decorrelation times varying between 0.322 and 0.780 s, for $S_4 = 1.0 \pm 0.025$ and $S_4 = 0.3 \pm 0.025$, respectively.

With respect to mid-latitude scintillation, Ledvina et al. (2004) presented estimates of the decorrelation times of the scintillation event they recorded at Cornell University (53.48°N dip lat). The site was located at much higher latitudes than UTD and they associated the observed scintillations with irregularities developing in a TEC depletion within a stom-enhanced density (SED) event (Foster, 1993). Examples of their observations show decorrelation times varying between ~0.25 and 2.0 s, with shorter decorrelation times observed in the equatorward edge of the TEC depletion (they call it trough), which were hypothesized to be linked to sub-auroral ionospheric drifts (SAIDs) or subauroral polarization streams (SAPs).

Therefore, the range of observed decorrelation times for the mid-latitude scintillation event of June 1st, 2013 coincides well with the range of values observed at low latitudes and associated with equatorial spread F, including those associated with intense amplitude fading ($S_4 > 0.8$). The decorrelation times are also in the same range of values observed during the mid-latitude event captured by Ledvina et al. (2004) and that was linked to SEDs.

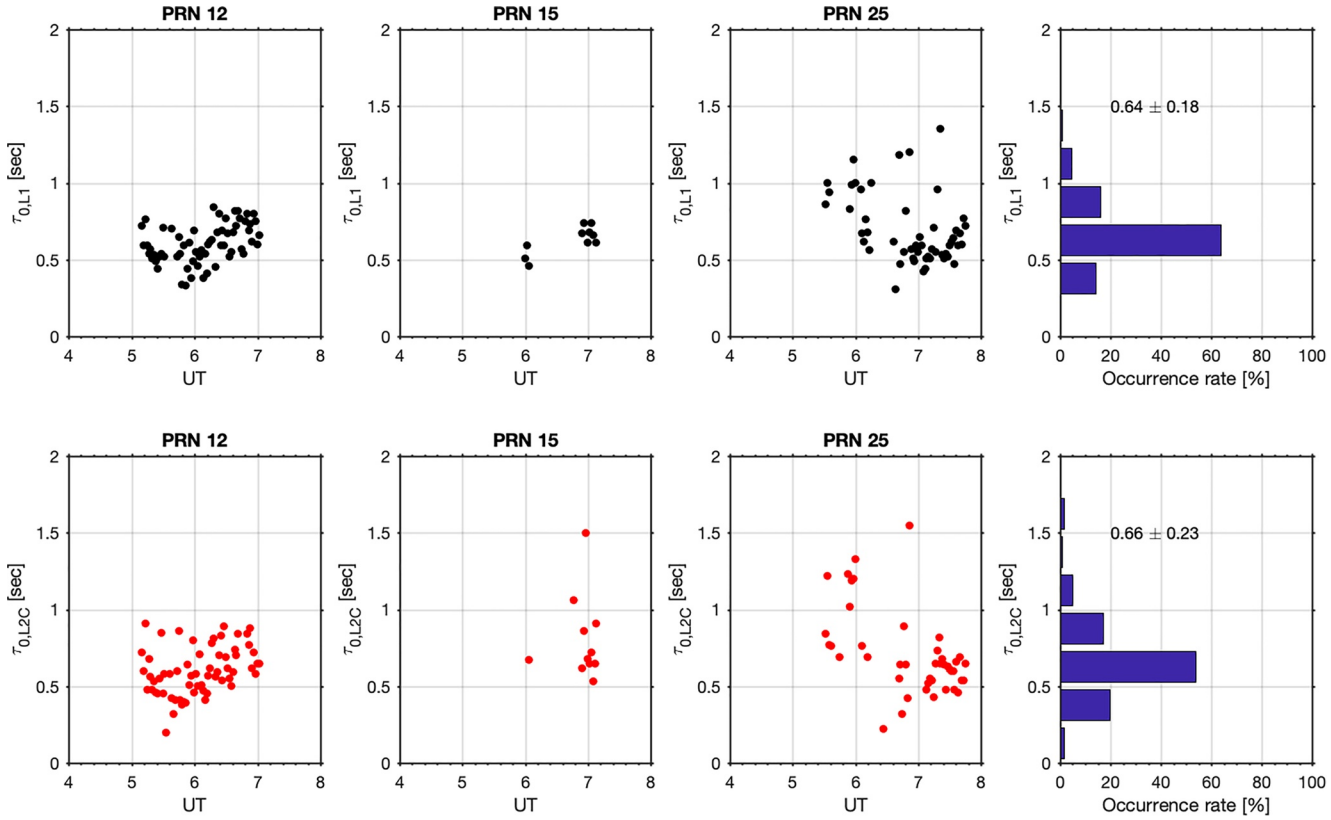

Figure 7. Observed decorrelation times for L1 (top panels) and L2C (bottom panels). The right-most panels in each row show the distribution of all observed values. Occurrence rate (in %) refers to the number of cases in each decorrelation time bin relative to the total number of cases. The average and standard deviation of the distributions are indicated for each distribution.

3.3. On Frequency Scaling of Scintillation Severity

The top panels of Figure 5 show that the L2C signal is more severely affected by ionospheric irregularities than the L1 signal. This is not unusual, and it was expected from previous observations and theoretical studies showing that scintillation has a frequency dependence (Yeh & Liu, 1982).

The frequency dependence of scintillation is important from two aspects. First, proper modeling of the frequency dependence would allow the intensity of scintillations observed in one frequency to be scaled to other frequencies. Second, determining the frequency dependence is also important for a fundamental understanding of the behavior of ionospheric irregularities since the scaling can be related to the spectrum of density perturbations responsible for the scintillations. For instance, theory for weak scattering can show that the S_4 index has a f^{-n} dependence, where f is the frequency of the signal, $n = \left(p + 3\right) / 4$, and p is the two-dimensional spectral slope of irregularities in the phase-changing screen model responsible for the scintillations (Franke et al., 1984; Rino, 1979).

The dual-frequency observations made by the CASES receivers provide an opportunity not only for concurrent TEC measurements, but also to evaluate frequency scaling of scintillation during a mid-latitude event.

Figure 8 now shows results of an analyses of the frequency scaling of S_4 as well as σ_ϕ for the mid-latitude event of June 1st, 2013 using L1 and L2C observations. The left panel shows the relationship between S_4 at L1 and L2C frequencies. The right panel shows the relationship for σ_ϕ at these two frequencies for the observations available. We only considered cases where $S_{4,L1} > 0.1$. The markers represent the measurements, which despite being limited in number, indicate a linear relationship between measurements at L1 and L2C. The solid red line represents least-square fits of linear models to the measurements. Expressions for the linear models are also presented in each panel, and show that $S_{4,L2C} \sim 1.28\, S_{4,L1}$ and $\sigma_{\phi,L2C} \sim 1.25\, \sigma_{\phi,L1}$.

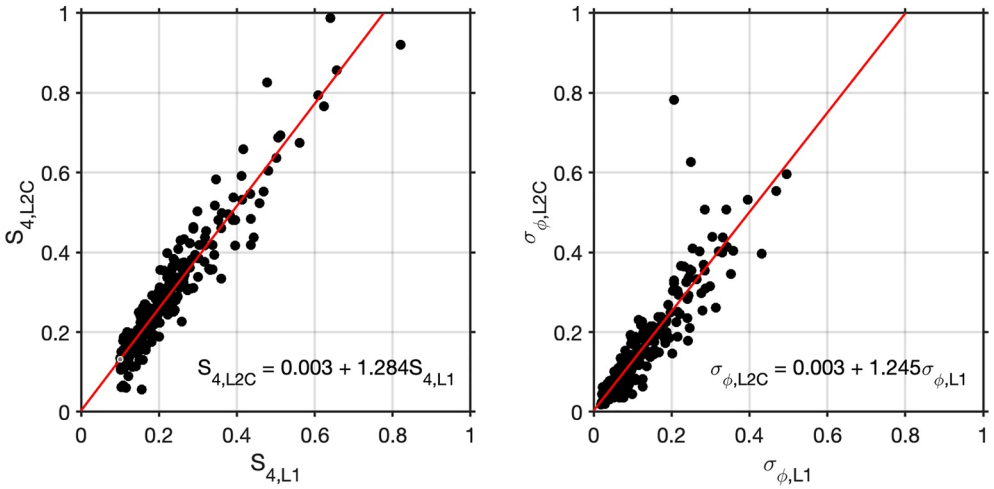

Figure 8. Left: The black markers show the observed relationship between the $S_{4,L1}$ and $S_{4,L2C}$ values measured in the signals from PRNs 12, 15, and 25. The red line represents a linear model that best fit the measurements. An expression for the best-fit model is also indicated. (b) Relationship between $\sigma_{\phi,L1}$ and $\sigma_{\phi,L2C}$ values measured in the signals from PRNs 12, 15, and 25. Again, the red line represents a linear model that best fit the measurements. Only measurements causing $S_{4,L1} > 0.1$ were considered.

The linear relationship found for the mid-latitude event described here is similar to what has been reported in the past, based mainly on observations made at low and high latitudes (Fremouw et al., 1978). In fact, $f^{-1.5}$ and f^{-1} dependencies for S_4 and σ_ϕ, have been recommended for scaling scintillation measurements made by single-frequency receivers (Van Dierendonck et al., 1993). For the case of L1 and L2C, these relationships translate to $S_{4,L2C} \sim 1.45\, S_{4,L1}$ and $\sigma_{\phi,L2C} \sim 1.24\, \sigma_{\phi,L1}$.

Furthermore, Carrano et al. (2014) pointed out that the assumptions upon which the frequency dependency was derived are not overly restrictive for GPS L-Band observations. Using GPS L1 and L2 scintillation observations made in Sao Jose dos Campos, Brazil near the equatorial anomaly peak and between October, 2012 and February, 2013, they found a linear relationship between $S_{4,L1}$ and $S_{4,L2C}$ to hold fairly well for a wide range of scintillation magnitudes including severe scintillation cases.

Additionally, Jiao and Morton (2015) analyzed S_4 and σ_ϕ indices measured at three different GPS frequencies (L1, L2, and L5) with receivers installed at three different sites, one located near the magnetic equator, one at low-latitudes and one at high latitudes. For the particular case of L1 and L2C measurements, they showed examples of measurements (single PRN for each latitude) with slopes varying between 1.16 and 1.45 for S_4 and 1.24 and 1.38 for σ_ϕ.

Finally, the study carried out by Moraes et al. (2017) used a large data set (5 months) of low-latitude GPS scintillation measurements and evaluated the relationship between S_4 and σ_ϕ measured at different frequencies. For L1 and L2C, in particular, they found that $S_{4,L2C} \sim 1.45\, S_{4,L1}$ (Fremouw et al., 1978) holds very well for $S_{4,L1} < 0.6$. For larger S_4 values, however, the linear relationship breaks down and a saturation effect was observed. They also found that the linear relationship for phase scintillation ($\sigma_{\phi,L2C} \sim 1.24\, \sigma_{\phi,L1}$), proposed by Fremouw et al. (1978) described well the behavior of their measurements for a wide range of σ_ϕ values (up to $\sim$ 1.4 rads).

Therefore, our analyses show the frequency dependence for both amplitude and phase scintillations observed in L1 and L2C signals during the mid-latitude event of June 1st, 2013. More importantly, it shows a linear relationship between scintillation indices observed in L1 and L2C that extends beyond the range of weak scintillation, which was also observed in observations made at low and high latitudes (Carrano et al., 2014; Jiao & Morton, 2015). While the saturation effect for $S_{4,L1} > 0.6$ reported by Moraes et al. (2017) does not seem to appear in our measurements, this could be at least in part due to the limited number of cases of strong amplitude scintillation in L1 caused by the mid-latitude event.

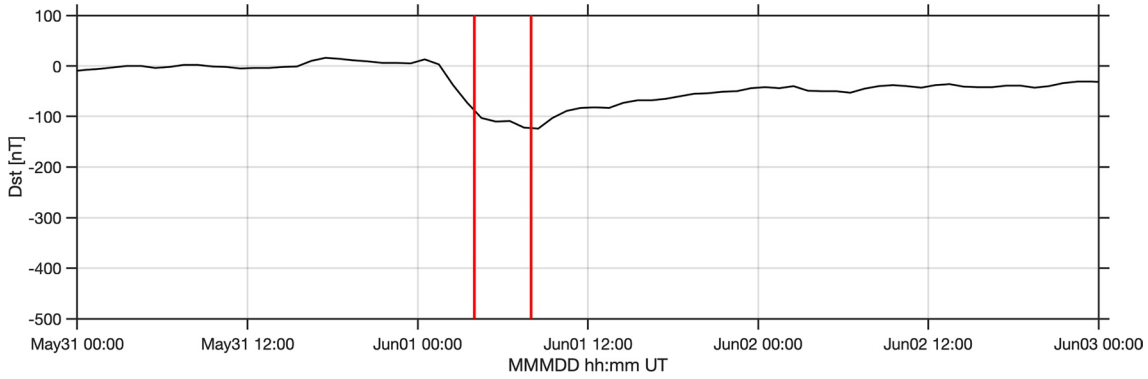

Figure 9. Geomagnetic conditions for May 31–June 2, 2013. The period under which scintillations were observed over UTD (June 1, 04:00–08:00 UT) is indicated by two vertical red lines.

3.4. On the Geospace Conditions Leading to the Observed Scintillation Event

We now provide information about the geomagnetic conditions under which the scintillation events of June 1st, 2013 were observed. Then, we discuss the large-scale (continental) behavior of the mid-latitude ionosphere over the US based on GPS TEC maps. Finally, we revisit some of the concurrent, nearly collocated optical observations of Martinis et al. (2015), which provide additional information about the underlying ionospheric structuring conditions leading to the scintillation event of June 1st.

3.4.1. On the Geomagnetic Conditions

Most reports of mid-latitude scintillation related the events to geomagnetically disturbed conditions (Afraimovich et al., 2009; Jean et al., 2017; Ledvina et al., 2002; Mrak et al., 2020; Rodrigues et al., 2004; Spogli et al., 2009). These reports, in general, related the occurrence of mid-latitude scintillation with the expansion of the auroral oval and irregularities associated with it to lower latitudes during geomagnetic storms. The event we report was also observed during a geomagnetically disturbed period. Figure 9 shows the temporal behavior of the Dst index between May 31st and June 3, 2013. The vertical red lines indicate the period (04:00–0800 UT of June 1st) in which scintillations were observed. This period coincides with the main phase of a moderate magnetic storm.

Of particular relevance here again is the study of Ledvina et al. (2002), which reported the first observations of intense GPS L1 amplitude scintillations at mid-latitudes. They captured the event with a scintillation monitor installed in the Northeastern part of the US and associated the scintillation-producing irregularities with a storm-enhanced density (SED) structure (Vo & Foster, 2001). The strongest scintillations observed by Ledvina et al. (2002) occurred in a region of large TEC gradients.

Like the event reported by Ledvina et al. (2002), the mid-latitude scintillations we present here occurred during the main phase of a moderate storm. In both cases, the Dst index reached a minimum of approximately −110 nT. The UTD site, however, is located in the southern part of the US, more than 10° of dip lat south of Ithaca, and expected to be outside the reach of an expanded auroral oval and mid-latitude trough even during a moderate magnetic storm.

3.4.2. On the Ionospheric Conditions Over the US

To assist with a better understanding of the large-scale (regional) ionospheric conditions leading to the observed scintillations, we take advantage of vertical TEC (VTEC) maps over the US obtained from the Madrigal database (http://cedar.openmadrigal.org). The TEC maps are created by the MIT Haytrack Observatory using observations made by dual-frequency GNSS receivers distributed over the US and globally. More details about these maps are provided in Rideout and Coster (2006). Here, it is sufficient to say that these maps provide snapshots of the spatial distribution of VTEC over the region of interest, that is, the southern United States. The spatial resolution of the maps is 1° in both latitude and longitude. The temporal resolution is 5 min.

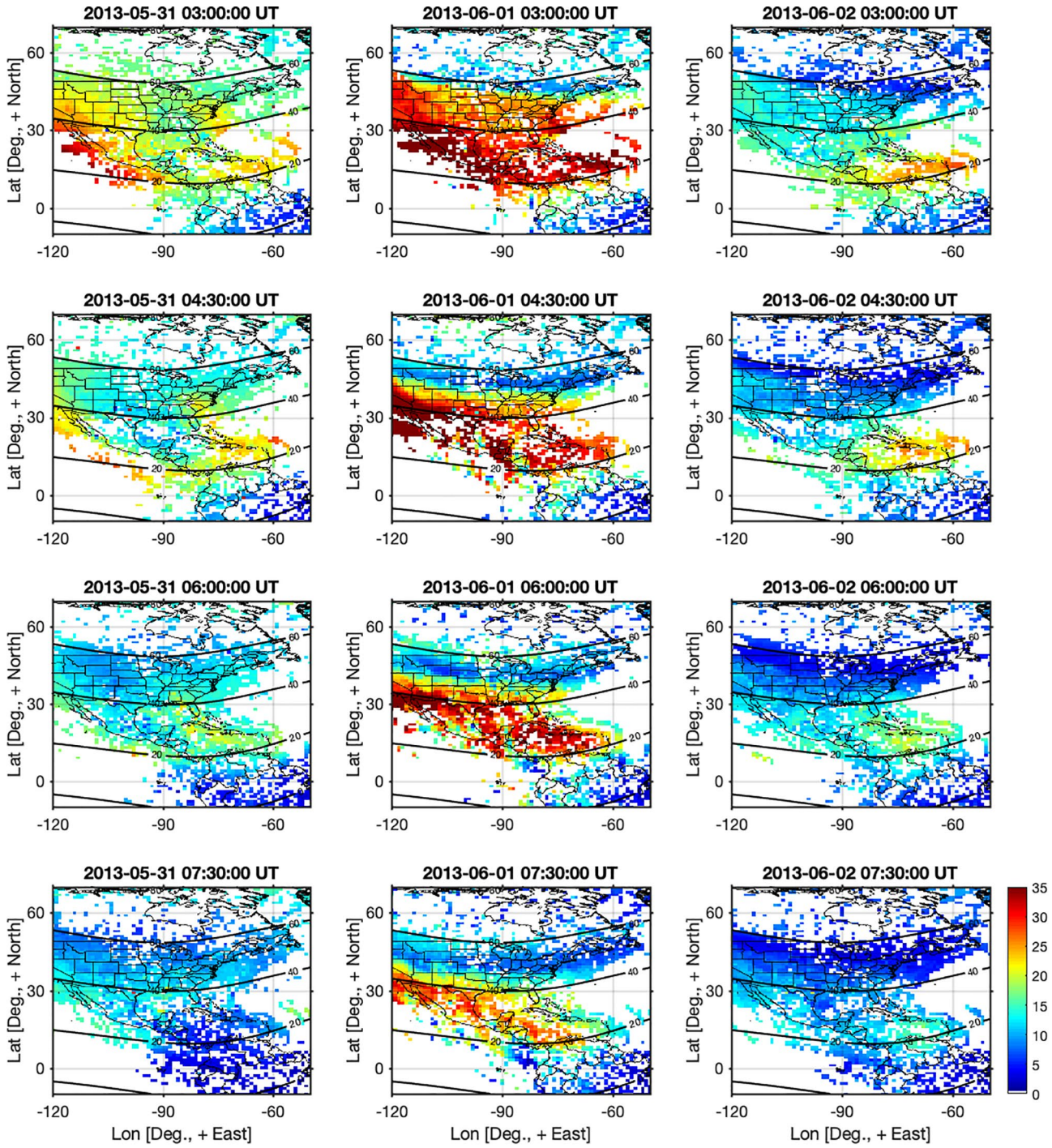

Figure 10. Snapshots of the vertical ionospheric total electron content (TEC) over the American sector for four different UT times (rows) on May 31 (left column), June 1 (middle column), and June 2, 2013 (right column). The color scale represents TEC units (TECU), and 1 TECU = 10^{16} el m^{-2}.

Figure 10 shows the behavior of TEC over the US for May 31–June 2, 2013. The central column of Figure 10 shows snapshots of VTEC over the American sector for four distinct times (03:00, 04:30, 06:00, and 07:30 UT) on June 1, 2013. For comparison purposes, the left and right columns show VTEC maps for the same times, but for the previous and following day, respectively. Regions in white indicate lack of data, which is mostly seen over the ocean where GNSS receivers are not deployed. Contours of dip latitude are also shown for reference.

Figure 10 serves to show at least a couple of important points. First, it shows that an enhancement in the background TEC can be observed over the US on June 1st. The background TEC values are much larger than the ones observed around the same time on other days. Here, it must be pointed out that the severity of amplitude scintillation increases with the absolute amplitude of the ionospheric plasma perturbations (e.g., Basu et al., 1976). Therefore, the depletions seen on June 1st, 2013 occur under enhanced background ionospheric densities, which favor the occurrence of large density perturbations and the observed strong scintillation events. This is similar to what happens at low latitudes where the latitudinal band around the equatorial anomaly peaks provide elevated ionospheric densities and favorable conditions for strong scintillations when ESF depletions develop (e.g., de Paula et al., 2003). The second point worth mentioning is that Figure 10 shows an equatorward motion of the ionospheric trough beyond what one would have expected even for moderately disturbed geomagnetic conditions. The region of reduced TEC associated with the trough can be seen as far as 45°N dip lat at 07:30 UT. This movement of the trough causes large latitudinal TEC gradients over the southernmost region of the US including Texas.

Additionally, the maps also seem to suggest that density depletions exist within the region of enhanced TEC. The spatial resolution of the maps, however, does not allow us to adequately resolve them. Fortunately, an all-sky camera was operating at the McDonald Observatory (30.67°N, 104.02°W, 39.31°N dip lat) with a field of view that covered the ionospheric region over our site and captured the behavior of the 630.0 nm nightglow emission (Martinis et al., 2015).

The all-sky camera provides information about ionospheric structuring with higher spatial resolution than it is possible to obtain with the TEC maps.

3.4.3. On Ionospheric Structuring Over Southern US

The observations made by an all-sky airglow imager operated at the McDonald Observatory during the geomagnetic storm of June 1st, 2013 were first presented and discussed by Martinis et al. (2015). They all-sky camera made measurements using a narrowband filter centered at 630.0 nm. The typical airglow structures observed at the McDonald Observatory are associated with medium-scale traveling disturbances (MSTIDs). On June 1st, 2013, however, it detected airglow signatures of high-latitude features (SAR arc) moving equatorward and the occurrence of airglow depletions that resemble those caused by equatorial plasma bubbles. In fact, Martinis et al. (2015) hypothesized that the airglow depletions were the manifestation of ESF structures that reached magnetic apex heights as high as 7,000 km and that mapped along magnetic field lines to mid latitudes. There have been several reports of late evening and post-midnight ESF events during June solstice under low solar flux conditions (e.g., Li et al., 2011; Otsuka, 2018; Patra et al., 2009; Yokoyama et al., 2011; Zhan et al., 2018) and reports of ESF associated with geomagnetic storms (e.g., Aarons, 1991; Fejer et al., 1999; Sahai et al., 2004; Tulasi Ram et al., 2008). The occurrence of ESF structures reaching as far as 7,000 km altitude (40° dip latitude) as proposed by Martinis et al. (2015), however, was unique.

Using observations from the C/NOFS and DMSP satellites, Martinis et al. (2015) confirmed the occurrence of ESF in the Pacific/North-American sector during the period. The DMSP satellite observations, however, were only available prior to the mid-latitude airglow observations. The observations also only showed the occurrence of depletions at lower latitudes, presumably, prior to its development to higher altitudes and latitudes. The C/NOFS observations show ESF signatures around the same time of the airglow depletions. These observations, however, were limited to lower latitudes. Finally, Martinis et al. (2015) pointed out that the airglow observations also showed signatures of a SAR arc moving equatorward. Using a TEC map, they also showed that the SAR arc was accompanied by the displacement of the trough to southern part of the US. The observations led Martinis et al. (2015) to suggest that the observed geospace activity was the manifestation of a convergence of the equatorial and auroral ionospheres. Our TEC maps (Figure 10) confirm the equatorward movement of the trough and highlight the unusual behavior of the mid-latitude ionosphere on June 1st compared to other days.

A comment by Kil et al. (2016), however, provided an alternative explanation for the optical observations. They suggested that the airglow depletions were the manifestation of mid-scale traveling ionospheric disturbances (MSTIDs). Their hypothesis was motivated, in particular, by the westward tilt of the airglow perturbations, which follows the pattern of MSTIDs observed at mid-latitudes in the past (Mendillo et al., 1997;

Otsuka et al., 2004). They also noted the existence of previous observations of "super-MSTIDs" (Nishioka et al., 2009) capable of causing TEC variations with large (>10 TECU) peak-to-peak amplitudes.

Here, we revisit the airglow observations to confirm the extent of which our scintillations were associated with the event captured by the airglow observations reported by Martinis et al. (2015). The airglow measurements were spaced by ~10 min and were made using a total exposure time of 120 s for the red line (630.0 nm) emission. Figure 11 shows snapshots of the airglow measurements from about 03:30 UT to about 08:30 UT on June 1st, 2013. The time is indicated on top of each panel.

In order to correlate the scintillation events with the airglow depletions, we plotted the IPPs of the GPS signals tracked by the UT Dallas receiver on the airglow images. The color of the tracks indicate the severity of amplitude scintillation in the L2C signal. Green indicates $S_{4,L2C} < 0.15$ and red indicates $S_{4,L2C} > 0.15$. The PRN is indicated for each track. To best match radio and optical observations, the tracks are for a period of 20 min total centered around the images shown.

Figure 11 shows that scintillation ($S_{4,L2C} > 0.15$) occurs mostly to the south of the site and, therefore, cannot be associated to irregularities, if any, within the trough or within the large-scale latitudinal density gradients that propagated from higher latitudes as shown by the TEC maps (Figure 10).

More importantly, scintillation occurred when the IPPs intercepted or were close to the darkest airglow bands, that is, to the airglow depletions that were associated to ESF by Martinis et al. (2015). Additionally, as shown earlier (Figure 4), scintillations occurred within TEC depletions. Therefore, Figure 11 also shows that the regions of low airglow emission are well correlated with the TEC depletions detected by the UTD CASES receiver. Using data from a single GPS receiver (dual-frequency but low rate sampling rate) installed at the McDonald Observatory, Martinis et al (2015) also found large VTEC fluctuations during the occurrence of the airglow perturbations that were comparable to those seen during strong ESF events.

We must point out that the airglow projections onto the map assume the nominal peak emission height of 300 km, which is the same height used by Martinis et al. (2015) in their analyses. The IPP coordinates were computed assuming a mean F-region peak height of 450 km instead of the nominal 350 km height that is commonly used in GNSS-based ionospheric studies. For high elevation satellites, the choices of either 350 or 450 km have no impact in the resulting IPP coordinates. For low elevation satellites, however, the choice of 450 km led to a better correlation between scintillation (or TEC depletions) and the darkest bands in airglow. This is the case, for instance, of the measurements made by PRN 24 on snapshots for 03:53 UT and 04:14 UT. Here, we must clarify that our assumption of the mean F-region peak height might not reflect the true height of the F-layer. This height could be affected by uncertainties in the assumption for the airglow emission height and by a displacement of the height of the irregularity layer with respect to the mean F-region peak.

4. Summary and Concluding Remarks

We reported a mid-latitude scintillation event that was captured by a GPS-based dual-frequency (L1 and L2C) scintillation monitor installed at UTD (32.99°N, 96.76°W, 43.2° dip latitude). The monitor has been used sporadically by undergraduate students for hands-on projects related to space weather, and this is the strongest scintillation event we were able to identify so far in our observations.

Perhaps more importantly, this event was observed at a "true" mid-latitude location where neither low nor high-latitude ionospheric phenomena were expected to be observed under quiet or even moderate geomagnetically disturbed conditions. Most of previous observations of mid-latitude scintillation were made at higher latitudes and associated with the equatorward expansion of the auroral oval (Afraimovich et al., 2009; Jean et al., 2017; Ledvina et al., 2002; Rodrigues et al., 2004; Spogli et al., 2009). Additionally, the observations captured cases of moderate-to-strong amplitude scintillation in the L2C signal.

The observations and analyses showed severe scintillation and TEC depletions occurring over southern US. For elevation angles greater than 30°, amplitude scintillation is mostly weak, that is, $S_4 < \sim 0.4$ in L1 and L2C. For elevation angles below about 30°, however, moderate ($S_4 > \sim 0.4$) scintillation events were observed in both L1 and L2C signals, and severe ($S_4 > \sim 0.8$) events were detected in the L2C signal.

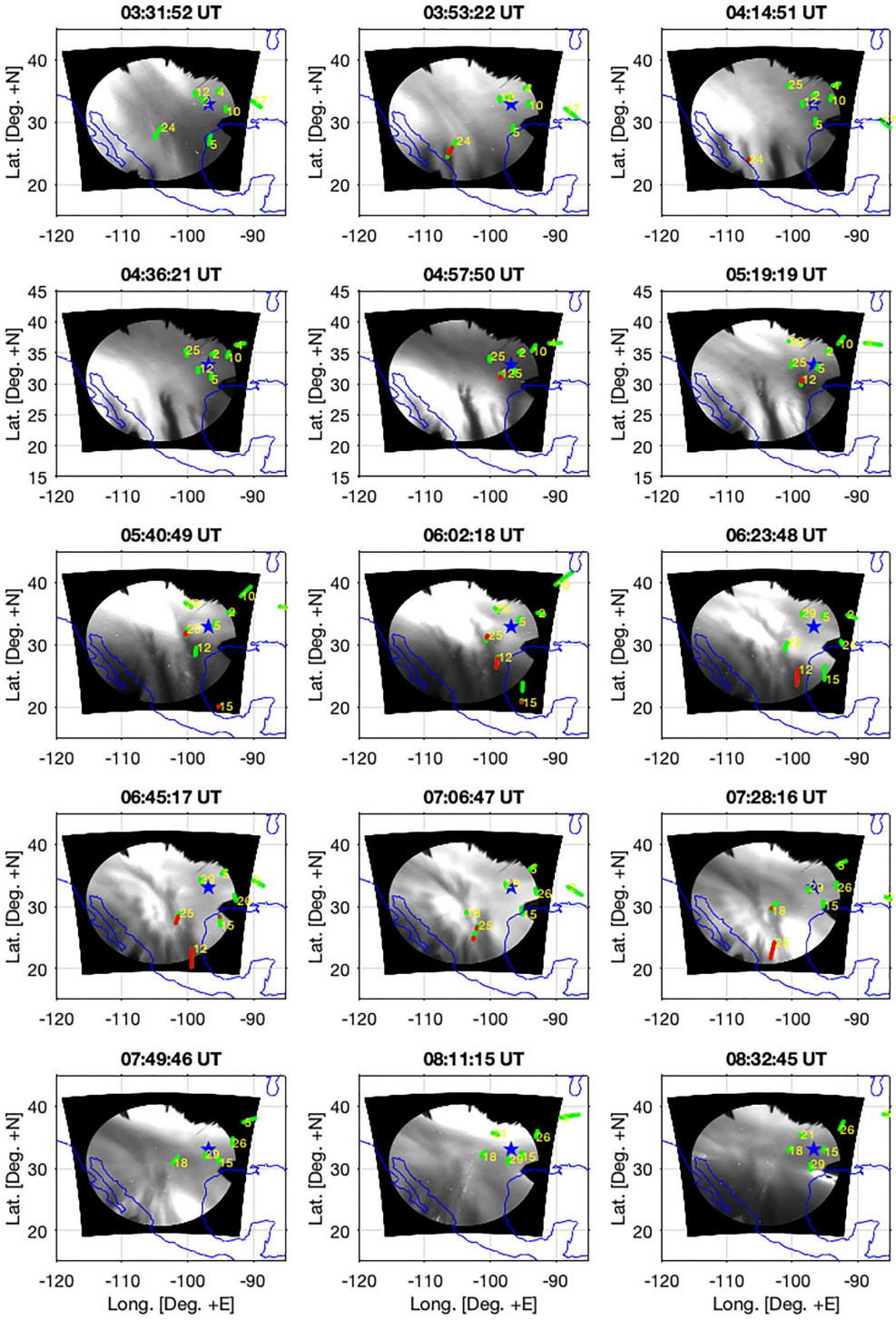

Figure 11. Snapshots of 630.0 nm airglow observations detected on June 1st, 2013 by an all-sky airglow imager located at the McDonald Observatory (30.67°N, 104.02°W, 39.31° dip lat). Tracks of the ionospheric piercing points (IPPs) of signals transmitted by GPS satellites and received by a GPS receiver located at UTD are also overlaid on the map as green markers. Red markers indicate the occurrence of amplitude scintillation observed on L2C signal ($S_{4,L2C} > 0.15$). The blue star indicates the location of the UTD receiver.

Amplitude scintillation was accompanied by phase scintillation with maximum σ_ϕ values exceeding 0.5 radians in L2C. We also found that the observed phase scintillations increased with amplitude scintillation severity, which is similar to what has been reported in studies of low-latitude scintillation. We pointed out that the observed scintillation magnitudes were severe even when compared to low-latitude scintillations observed during similar solar flux conditions (e.g., Moraes et al., 2017).

We also reported the observed rapidity of the observed amplitude scintillations. Decorrelation times varied mostly between 0.25 and 1.25 s, with a mean value around 0.65 s for both L1 and L2C signals. While the time scales are similar to those seen in low-latitude scintillations (e.g., Carrano & Groves, 2010; Moraes et al., 2013), they are also within the range of values reported by Ledvina et al. (2004) during another scintillation event observed at higher latitudes.

The availability of measurements in two frequencies allowed us to investigate the frequency scaling of amplitude scintillation. The observations matched fairly well the predictions for weak scattering, that is, $S_4 \propto f^{-n}$. The observations also showed that theoretical predictions were not overrestrictive and extended to high S_4 values, similar to what was observed by Carrano et al. (2014) using GPS observations made at low latitudes and Jiao and Morton (2015) at low and high latitudes. We must point out that Moraes et al. (2017), however, found using a large set of low-latitude observations that $S_{4,L2}$ tend to saturate during events causing high $S_{4,L1}$ values.

We also examined the geomagnetic and ionospheric conditions leading to the observed scintillation event of June 1st, 2013. We found that the event occurred during the main phase of a moderate magnetic storm, when the Dst index reached a minimum of −110 nT. GPS-derived TEC maps, allowed us to verify that the magnetic storm, despite being moderate, prompted the equatorward movement of the mid-latitude trough as far as 45° dip latitude, the development of impressive background TEC enhancements and large TEC depletions over the United States. The enhanced background ionospheric densities created conditions that favored the occurrence of intense scintillation within the TEC depletions, similar to what is observed near the equatorial anomaly peaks during the occurrence of equatorial plasma bubbles.

Additionally, we identified that scintillations occurred within the same ionospheric depletions captured by an all-sky airglow camera at the McDonald Observatory in Texas, and that were reported by Martinis et al. (2015). In addition to an expansion of the auroral oval, the camera also detected signatures of large ionospheric depletions that were very similar to those produced in airglow images by low-latitude ionospheric plasma bubbles. Martinis et al. (2015) hypothesized that the airglow observations were produced by a "super ESF" event that reached over 7,000 km in apex altitude and, therefore, magnetic latitudes over southern US. Kil et al. (2016) provided an alternative explanation, in which the airglow observations could have been produced by a "super MSTID".

Finally, the properties of the observed scintillation events show a remarkable resemblance to those of low-latitude ESF measurements. This corroborates with the hypothesis of a link of the airglow depletions with the so-called super ESF events. Here, it is important to add an important piece of information provided by the work of Aa et al. (2019), which analyzed another event showing large ionospheric depletions over southern United States on September 7, 2017. Of particular relevance is the fact that these perturbations were also observed during a moderate geomagnetic storm (minimum Dst reached −124 nT). More importantly, they presented TEC maps available for the American sector that show clear signatures of TEC depletions developing from low latitudes and reaching the southern portion of the US (apex latitudes as high as 6,800 km). This provides additional experimental evidence that super ESF events could occur and reach the US more often than expected.

While additional work needs to be carried out to address the origin of the mid-latitude ionospheric disturbances observed over the US, this study contributes with details about the properties of and geospace conditions associated with mid-latitude scintillations events over the US. Additionally, it contributes with observational evidence that space weather events can cause significant impact in the propagation of trans-ionospheric radio signals, including those in the frequency band used by GNSS receivers, at mid latitudes.

Data Availability Statement

Quick-look airglow images from the McDonald Observatory and other sites are available at http://sirius.bu.edu/dataview/. UTD scintillation and TEC measurements are available in a public data repository located at http://doi.org/10.5281/zenodo.4752071. TEC map data can be obtained from the Madrigal database (http://madrigal.haystack.mit.edu). GPSTEC data products and access through the Madrigal distributed data system are provided to the community by theMassachusetts Institute of Technology under support from US National Science Foundation grant AGS-1952737. Data for the TEC processing is provided from the following organizations: UNAVCO, Scripps Orbit and Permanent Array Center, Institut Geographique National, France, International GNSS Service, The Crustal Dynamics Data Information System (CDDIS), National Geodetic Survey, Instituto Brasileiro de Geografia e Estatística, RAMSAC CORS of Instituto Geográfico Nacional de la República Argentina, Arecibo Observatory, Low-Latitude Ionospheric Sensor Network (LISN), Topcon Positioning Systems, Inc., Canadian High Arctic Ionospheric Network, Institute of Geology and Geophysics, Chinese Academy of Sciences, China Meteorology Administration, Centro di Ricerche Sismologiche, Système d'Observation du Niveau des Eaux Littorales (SONEL), RENAG: REseau NAtional GPS permanent, GeoNet - the official source of geological hazard information for New Zealand, GNSS Reference Networks, Finnish Meteorological Institute, SWEPOS - Sweden, Hartebeesthoek Radio Astronomy Observatory, TrigNet Web Application, South Africa, Australian Space Weather Services, RETE INTEGRATA NAZIONALE GPS, Estonian Land Board, Virginia Tech Center for Space Science and Engineering Research, and Korea Astronomy and Space Science Institute.

Acknowledgments
GPS data collection was supported by UTD's faculty start-up funds to FSR. Processing and analyses were supported by NSF (Award AGS-1554926) and NASA (Award 80NSSC18K1203). A.O. Moraes was supported by CNPq award number 314043/2018-7. Some of this research was performed while D.A. Hickey held an NRC Research Associateship award at the US Naval Research Laboratory. D.A. Hickey's work is supported by the United States Chief of Naval Research (US CNR).

References

Aa, E., Huang, W., Liu, S., Ridley, A., Zou, S., Shi, L., et al. (2018). Midlatitude plasma bubbles over China and adjacent areas during a magnetic storm on 8 September 2017. *Space Weather*, *16*, 321–331. https://doi.org/10.1002/2017SW001776

Aa, E., Zou, S., Ridley, A., Zhang, S., Coster, A. J., Erickson, P. J., et al. (2019). Merging of storm time midlatitude traveling ionospheric disturbances and equatorial plasma bubbles. *Space Weather*, *17*(2), 285–298. https://doi.org/10.1029/2018sw002101

Aarons, J. (1982). Global morphology of ionospheric scintillations. *Proceedings of the IEEE*, *70*, 360–378. https://doi.org/10.1109/proc.1982.12314

Aarons, J. (1991). The role of the ring current in the generation or inhibition of equatorial F layer irregularities during magnetic storms. *Radio Science*, *26*(4), 1131–1149. https://doi.org/10.1029/91RS00473

Aarons, J. (1997). 50 years of radio-scintillation observations. *IEEE Antennas and Propagation Magazine*, *89*, 6.

Afraimovich, E. L., Astafieva, E. I., Demyanov, V. V., & Gamayunov, I. F. (2009). Mid-latitude amplitude scintillation of GPS signals and GPS performance slips. *Advances in Space Research*, *43*, 964–972. https://doi.org/10.1016/j.asr.2008.09.015

Appleton, E. (1946). Two Anomalies in the Ionosphere. *Nature*, *157*, 691. https://doi.org/10.1038/157691a0

Basu, S., Basu, S., & Khan, B. K. (1976). Model of equatorial scintillations from in-situ measurements. *Radio Science*, *11*(10), 821–832. https://doi.org/10.1029/RS011i010p00821

Basu, S., Weber, E. J., Bullett, T. W., Keskinen, M. J., MacKenzie, E., Doherty, P., et al. (1998). Characteristics of plasma structuring in the cusp/cleft region at Svalbard. *Radio Science*, *33*(6), 1885–1899. https://doi.org/10.1029/98RS01597

Beach, T. L. (2006). Perils of the GPS phase scintillation index (s_f). *Radio Science*, *41*, RS5S31. https://doi.org/10.1029/2005RS003356

Beach, T. L., & Kintner, P. M. (1999). Simultaneous Global Positioning System observations of equatorial scintillations and total electron content fluctuations. *Journal of Geophysical Research*, *104*(A10), 22553–22565. https://doi.org/10.1029/1999JA900220

Bhattacharyya, A., Beach, T. L., Basu, S., & Kintner, P. M. (2000). Nighttime equatorial ionosphere: GPS scintillations and differential carrier phase fluctuations. *Radio Science*, *35*(1), 209–224. https://doi.org/10.1029/1999RS002213

Buchau, J., Weber, E. J., Anderson, D. N., Carlson, H. C., Moore, J. G., Reinisch, B. W., & Livingston, R. C. (1985). Ionospheric structures in the polar cap: Their origin and relation to 250-MHz scintillation. *Radio Science*, *20*(3), 325–338. https://doi.org/10.1029/RS020i003p00325

Bust, G. S., & Mitchell, C. N. (2008). History, current state, and future directions of ionospheric imaging. *Reviews of Geophysics*, *46*, RG1003. https://doi.org/10.1029/2006RG000212

Carrano, C. S., & Groves, K. M. (2010). Temporal decorrelation of GPS satellite signals due to multiple scattering from ionospheric irregularities. In *Proceedings of the 23rd international technical meeting of the Satellite division of the institute of navigation (ION GNSS 2010)*. (pp. 361–374). Portland, OR: Institute of Navigation.

Carrano, C. S., Groves, K. M., Delay, S. H., & Doherty, P. H. (2014). An inverse diffraction technique for scaling measurements of ionospheric scintillations on the GPS L1, L2, and L5 carriers to other frequencies. In *Proceedings of the 2014 international technical meeting of the institute of navigation*. (pp. 709–719). San Diego, CA: Institute of Navigation.

Cherniak, I., & Zakharenkova, I. (2016). First observations of super plasma bubbles in Europe. *Geophysical Research Letters*, *43*, 11137–11145. https://doi.org/10.1002/2016GL071421

Crowley, G., Bust, G. S., Reynolds, A., Azeem, I., Wilder, R., O'Hanlon, B. W., et al. (2011). CASES: A novel low-cost ground-based dual-frequency GPS software receiver and space weather monitor. In *Proceedings of the 24th international technical meeting of the satellite division of the institute of navigation*. (pp. 1437–1446). Manassas, VA: Institue of Navigation.

de Paula, E. R., Rodrigues, F. S., Iyer, K. N., Kantor, I. J., Abdu, M. A., Kintner, P. M., et al. (2003). Equatorial anomaly effects on GPS scintillations in Brazil. *Advances in Space Research*, *31*(3), 749–754. https://doi.org/10.1016/S0273-1177(03)00048-6

Deshpande, K. B., Bust, G. S., Clauer, C. R., Kim, H., Macon, J. E., Humphreys, T. E., et al. (2012). Initial GPS scintillation results from CASES receiver at South Pole, Antarctica. *Radio Science*, *47*(05), RS5009. https://doi.org/10.1029/2012RS005061

Erickson, P. E. (2020). Mid-latitude ionopsheric features: Natural complexity in action. In *The dynamic ionosphere* (ISBN: 9780128147825). (pp. 25–38). Elsevier. https://doi.org/10.1016/b978-0-12-814782-5.00005-4

Fejer, B. G., Scherliess, L., & de Paula, E. R. (1999). Effects of the vertical plasma drift velocity on the generation and evolution of equatorial spread F. *Journal of Geophysical Research*, *104*(A9), 19859–19869. https://doi.org/10.1029/1999JA900271

Foster, J. C. (1993). Storm time plasma transport at middle and high latitudes. *Journal of Geophysical Research*, *98*(A2), 1675–1689. https://doi.org/10.1029/92JA02032

Franke, S. J., Liu, C. H., & Fang, D. J. (1984). Multifrequency study of ionospheric scintillation at Ascension Island. *Radio Science*, *19*(3), 695–706. https://doi.org/10.1029/RS019i003p00695

Fremouw, E. J., Leadabrand, R. L., Livingston, R. C., Cousins, M. D., Rino, C. L., Fair, B. C., & Long, R. A. (1978). Early results from the DNA Wideband satellite experiment—Complex-signal scintillation. *Radio Science*, *13*(1), 167–187. https://doi.org/10.1029/RS013i001p00167

Humphreys, T. E., Psiaki, M. L., Ledvina, B. M., Cerruti, A. P., & Kintner, P. M. (2010). Data-driven testbed for evaluating GPS carrier tracking loops in ionospheric scintillation. *IEEE Transactions on Aerospace and Electronic Systems*, *46*(4), 1609–1623. https://doi.org/10.1109/TAES.2010.5595582

Hysell, D., Larsen, M., Fritts, D., Laughman, B., & Sulzer, M. (2018). Major upwelling and overturning in the mid-latitude F region ionosphere. *Nature Communications*, *9*, 3326. https://doi.org/10.1038/s41467-018-05809-x

Jean, M. H., Conroy, J. P., & Scales, W. A. (2017). *Multi-constellation GNSS scintillation at mid-latitudes*. (Vol. 32, pp. 19–26). Montreal: URSI GASS.

Jiao, Y., & Morton, Y. T. (2015). Comparison of the effect of high-latitude and equatorial ionospheric scintillation on GPS signals during the maximum of solar cycle 24. *Radio Science*, *50*, 886–903. https://doi.org/10.1002/2015RS005719

Kil, H., Miller, E. S., Jee, G., Kwak, Y. S., Zhang, Y., Nishioka, M., et al. (2016). Comment on "The night when the auroral and equatorial ionospheres converged" by C. Martinis, J. Baumgardner, M. Mendillo, J. Wroten, A. Coster, and L. Paxton. *Journal of Geophysical Research: Space Physics*, *121*, 10599–10607. https://doi.org/10.1002/2016JA022662

Kintner, P. M., Jr, Coster, A. J., Fuller-Rowell, T., Mannucci, A. J., Mendillo, M., & Heelis, R. (2008). Midlatitude ionospheric dynamics and disturbances: Introduction. In P. M. Kintner, A. J. Coster, T. Fuller-Rowell, A. J. Mannucci, M. Mendillo, & R. Heelis (Eds.), *Midlatitude ionospheric dynamics and disturbances* (pp. 1–7). AGU. https://doi.org/10.1029/181GM02

Kintner, P. M., Kil, H., Beach, T. L., & de Paula, E. R. (2001). Fading timescales associated with GPS signals and potential consequences. *Radio Science*, *36*(4), 731–743. https://doi.org/10.1029/1999RS002310

Kintner, P. M., Ledvina, B. M., & de Paula, E. R. (2007). GPS and ionospheric scintillations. *Space Weather*, *5*, S09003. https://doi.org/10.1029/2006SW000260

Komjathy, A. (1997). Global ionospheric total electron content mapping using the global positioning system (Ph.D. dissertation). (p. 248). Fredericton, New Brunswick, Canada: Department of Geodesy and Geomatics Engineering Technical Report No. 188, University of New Brunswick.

Laundal, K. M., & Richmond, A. D. (2017). Magnetic coordinate systems. *Space Science Reviews*, *206*, 27–59. https://doi.org/10.1007/s11214-016-0275-y

Ledvina, B. M., Kintner, P. M., & Makela, J. J. (2004). Temporal properties of intense GPS L1 amplitude scintillations at midlatitudes. *Radio Science*, *39*, RS1S18. https://doi.org/10.1029/2002RS002832

Ledvina, B. M., Makela, J. J., & Kintner, P. M. (2002). First observations of intense GPS L1 amplitude scintillations at midlatitude. *Geophysical Research Letters*, *29*(14), 4–1. https://doi.org/10.1029/2002GL014770

Li, G., Ning, B., Abdu, M. A., Yue, X., Liu, L., Wan, W., & Hu, L. (2011). On the occurrence of postmidnight equatorial F region irregularities during the June solstice. *Journal of Geophysical Research*, *116*(A4), A04318. https://doi.org/10.1029/2010JA016056

Liu, Y., Li, Z., Fu, L., Wang, J., & Zhang, C. (2020). Studying the ionospheric responses induced by a geomagnetic storm in September 2017 with multiple observations in America. *GPS Solutions*, *24*, 3. https://doi.org/10.1007/s10291-019-0916-1

Luo, X., Gu, S., Lou, Y., Cai, L., & Liu, Z. (2020). Amplitude scintillation index derived from C/N 0 measurements released by common geodetic GNSS receivers operating at 1 Hz. *Journal of Geodesy*, *94*(2), 1–14. https://doi.org/10.1007/s00190-020-01359-7

Ma, G., & Maruyama, T. (2006). A super bubble detected by dense GPS network at East Asian longitudes. *Geophysical Research Letters*, *33*, L21103. https://doi.org/10.1029/2006GL027512

Martinis, C., Baumgardner, J., Mendillo, M., Wroten, J., Coster, A., & Paxton, L. (2015). The night when the auroral and equatorial ionospheres converged. *Journal of Geophysical Research: Space Physics*, *120*, 8085–8095. https://doi.org/10.1002/2015JA02155

Mendillo, M., Baumgardner, J., Nottingham, D., Aarons, J., Reinisch, B., Scali, J., & Kelley, M. (1997). Investigations of thermospheric-ionospheric dynamics with 6300-Å images from the Arecibo Observatory. *Journal of Geophysical Research*, *102*(A4), 7331–7343. https://doi.org/10.1029/96JA02786

Moraes, A. O., Costa, E., Abdu, M. A., Rodrigues, F. S., de Paula, E. R., Oliveira, K., & Perrella, W. J. (2017). The variability of low-latitude ionospheric amplitude and phase scintillation detected by a triple-frequency GPS receiver. *Radio Science*, *52*, 439–460. https://doi.org/10.1002/2016RS006165

Moraes, A. O., de Paula, E. R., Parrella, W. J., & Rodrigues, F. S. (2013). On the distribution of GPS signal amplitudes during low-latitude ionospheric scintillation. *GPS Solutions*, *17*, 4. https://doi.org/10.1007/s10291-012-0295-3

Mrak, S., Semeter, J., Nishimura, Y., Rodrigues, F. S., Coster, A. J., & Groves, K. (2020). Leveraging geodetic GPS receivers for ionospheric scintillation science. *Radio Science*, *55*, e2020RS007131. https://doi.org/10.1029/2020RS007131

Nishioka, M., Saito, A., & Tsugawa, T. (2009). Super-medium-scale traveling ionospheric disturbance observed at midlatitude during the geomagnetic storm on 10 November 2004. *Journal of Geophysical Research*, *114*, A07310. https://doi.org/10.1029/2008JA013581

O'Hanlon, B. W., Psiaki, M. L., Powell, S., Bhatti, J. A., Humphreys, T. E., Crowley, G., & Bust, G. S. (2011). CASES: A smart, compact GPS software receiver for space weather monitoring. In *Proceedings of the 24th international technical meeting of the satellite division of the institute of navigation* (pp. 2745–2753). Manassas, VA: Institute of Navigation.

Otsuka, Y. (2018). Review of the generation mechanisms of post-midnight irregularities in the equatorial and low-latitude ionosphere. *Progress in Earth and Planetary Science*, *5*, 57. https://doi.org/10.1186/s40645-018-0212-7

Otsuka, Y., Shiokawa, K., Ogawa, T., & Wilkinson, P. (2004). Geomagnetic conjugate observations of medium-scale traveling ionospheric disturbances at midlatitude using all-sky airglow imagers. *Geophysical Research Letters*, *31*, L15803. https://doi.org/10.1029/2004GL020262

Patra, A. K., Phanikumar, D. V., & Pant, T. K. (2009). Gadanki radar observations of F region field-aligned irregularities during June solstice of solar minimum: First results and preliminary analysis. *Journal of Geophysical Research*, *114*(A12), A12305. https://doi.org/10.1029/2009JA014437

Pi, X., Mannucci, A., Lindqwister, U., & Ho, C. (1997). Monitoring of global ionospheric irregularities using the worldwide GPS network. *Geophysical Research Letters*, *24*, 2283–2286. https://doi.org/10.1029/97gl02273

Rideout, W., & Coster, A. (2006). Automated GPS processing for global total electron content data. *GPS Solutions*, *10*, 219–228. https://doi.org/10.1007/s10291-006-0029-5

Rino, C. (1976). Ionospheric scintillation theory--A mini-review. *IEEE Transactions on Antennas and Propagation*, *24*(6), 912–915. https://doi.org/10.1109/TAP.1976.1141439

Rino, C. (1979). A power law phase screen model for ionospheric scintillation, 1 Weak scatter. *Radio Science*, *14*, 1135–1145. https://doi.org/10.1029/rs014i006p01135

Rodrigues, F. S., Aquino, M. H. O., Dodson, A., Moore, T., & Waugh, S. (2004). Statistical analysis of GPS ionospheric scintillation and short-time TEC variations over northern Europe. *Journal of the Institute of Navigation*, *51*(1), 59–75. https://doi.org/10.1002/j.2161-4296.2004.tb00341.x

Sahai, Y., Fagundes, P. R., Abalde, J. R., Pimenta, A. A., Bittencourt, J. A., Otsuka, Y., & Rios, V. H. (2004). Generation of large-scale equatorial F-region plasma depletions during lowrange spread-F season. *Annales Geophysicae*, *22*, 15–23. https://doi.org/10.5194/angeo-22-15-2004

Spogli, L., Alfonsi, L., De Franceschi, G., Romano, V., Aquino, M. H. O., & Dodson, A. (2009). Climatology of GPS ionospheric scintillations over high and mid-latitude European regions. *Annales Geophysicae*, *27*, 3429–3437. https://doi.org/10.5194/angeo-27-3429-2009

Sun, Y.-Y., Matsuo, T., Araujo-Pradere, E. A., & Liu, J.-Y. (2013). Ground-based GPS observation of SED-associated irregularities over CONUS. *Journal of Geophysical Research: Space Physics*, *118*, 2478–2489. https://doi.org/10.1029/2012JA018103

Thébault, E., Finlay, C. C., Beggan, C. D., Alken, P., Aubert, J., Barrois, O., et al. (2015). International Geomagnetic Reference Field: The 12th generation. *Earth Planets and Space*, *67*, 79. https://doi.org/10.1186/s40623-015-0228-9

Tulasi Ram, S., Rama Rao, P. V. S., Prasad, D. S. V. V. D., Niranjan, K., Gopi Krishna, S., Sridharan, R., & Ravindran, S. (2008). Local time dependent response of postsunset ESF during geomagnetic storms. *Journal of Geophysical Research*, *113*, A07310. https://doi.org/10.1029/2007JA012922

Van Dierendonck, A. J., Klobuchar, J., & Hua, Q. (1993). Ionospheric scintillation monitoring using commercial single frequency C/A code receivers. In *Proceedings of ION GPS-93*. (Vol. 93, pp. 1333–1342). Arlington, VA: Institute of Navigation.

Vo, H. B., & Foster, J. C. (2001). A quantitative study of ionospheric density gradients at midlatitudes. *Journal of Geophysical Research*, *106*(A10), 21555–21563. https://doi.org/10.1029/2000JA000397

Woodman, R. F. (2009). Spread F–An old equatorial aeronomy problem finally resolved? *Annales Geophysicae*, *27*, 1915–1934. https://doi.org/10.5194/angeo-27-1915-2009

Yeh, K. C., & Liu, C.-H. (1982). Radio wave scintillations in the ionosphere. *Proceedings of the IEEE*, *70*(4), 324–360. https://doi.org/10.1109/PROC.1982.12313

Yokoyama, T., Yamamoto, M., Otsuka, Y., Nishioka, M., Tsugawa, T., Watanabe, S., & Pfaff, R. F. (2011). On postmidnight low-latitude ionospheric irregularities during solar minimum: 1. Equatorial atmosphere radar and GPS-TEC observations in Indonesia. *Journal of Geophysical Research: Space Physics*, *116*(A11), A11325. https://doi.org/10.1029/2011JA016797

Zhan, W., Rodrigues, F., & Milla, M. (2018). On the genesis of postmidnight equatorial spread F: Results for the American/Peruvian sector. *Geophysical Research Letters*, *45*, 7354–7361. https://doi.org/10.1029/2018GL078822